Bulk and Interfacial Aqueous Fluoride: An Investigation via First Principles Molecular Dynamics†

Ming-Hsun Ho,‡ Michael L. Klein,‡ and I.−F. William Kuo*,§

Center for Molecular Modeling and Department of Chemistry, University of Pennsylvania, Philadelphia, Pennsylvania 19104-6323, Chemical Sciences Division, Lawrence Livermore National Laboratory, P.O. Box 808, Livermore, California 94551

Received: October 2, 2008; Revised Manuscript Received: December 31, 2008

Using first principles molecular dynamics simulation, we have studied a fluoride anion embedded in a periodically replicated water slab composed of 215 water molecules to mimic both bulk and interfacial solvation. In contrast to some recent experiments, our findings suggest that there are only small structural changes for fluoride and its first solvation shell in the bulk. Moreover, the presence of fluoride does not significantly alter the rotational dynamics of nearby water. In addition, we have computed the molecular dipole moments using Wannier centers. At the interface, the presence of fluoride increases the molecular dipole moments of nearby water molecules, whereas in the bulk, the dipole moments for water appear to be essentially invariant to the presence of fluoride in the vicinity. Previous studies of the air−water interface have showed interfacial water to have higher average HOMO energies and, thus, likely to be more prone to electrophilic attack. With the addition of fluoride, the most likely reactive site for electrophilic reactions shifts to the anion. This finding could explain the known large increase in reaction rates for heterogeneous process of interest in atmospheric science. The reactive properties of other anions near the air−water interface are of general interest in heterogeneous chemistry and can be elucidated using a similar type of analysis, as performed here for the fluoride anion.

I. Introduction

Hydrogen bonding fluids are associated with many important processes in natural sciences and have been studied extensively using molecular simulations. In particular, the resurgence of interest in the study of surface properties of electrolyte solutions, and especially liquid−vapor interfaces, has been stimulated by a flurry of experimental and theoretical studies.[1−17] Counter to the previous notion that the air−water interface is depleted of alkali halide ions, recent experiments have revealed population enhancements at the liquid−vapor interface. In addition, theoretical studies using classical polarizable interaction potentials have elucidated the effect of ion size and polarizability on surface enhancements at the liquid−vapor interface. The ramification of this increased concentration of alkali halide ions at the liquid−vapor interface is profound for the field of heterogeneous chemistry.[18,19] In comparison to our understanding of the structural and dynamical properties of electrolytic solutions at the liquid−vapor interface, the effects on electronic properties and chemical reactivity due to the presence of the alkali halide ions is relatively unexplored and is thus an area ripe for further investigation. One method to gain insight into chemical reactivity is to utilize electronic structure calculations in which ions are solvated in water clusters.[15,16] Unless clusters are large, insights gleaned by using a cluster approach cannot compensate for the anisotropic solvation of a true interface. This effect will become even more important with increasing size or polarizability of the solvated anions and thus influence its chemical reactivity. Accordingly, in this study, we will look at the effective change in structure, dynamics, and chemical reactivity at the interface in the presence of an anion using a water slab.

With recent advances in fast electronic structure algorithms and high-performance computing, it is now possible to investigate the neat liquid−vapor interface using first principles molecular dynamics (MD) simulation based on density functional theory (DFT).[20−22] Prior studies have shown that DFT using gradient-corrected functionals such as Becke−Lee−Yang−Parr (BLYP)[23,24] or the Perdew−Burke−Ernzerhof (PBE)[25] exchange and correlation functional can be useful in interpreting measurements on an aqueous system, including surface sensitive experiments. One glaring problem with the use of DFT based schemes, as usually applied, is the failure to correctly predict the density of hydrogen bonded fluids (i.e., water and methanol) when either BLYP or PBE exchange and correlation functionals are utilized. The predicted low density of hydrogen bonded fluid is possibility due to the lack of London dispersion forces in usual DFT schemes.[26,27]

Attempts to elucidate surface affinities of ions using DFT have previously relied on short-duration MD simulations that can only offer qualitative behavior of ion affinity toward the interface.[28,29] Although computationally expensive, it is possible to utilize DFT-based MD simulations and compute the potential of mean force for moving an ion across the air−water interface and thus determine the ion surface affinity. Such an attempt to compute the potential of mean force has shown fluoride is repelled from the air−water interface, a finding that is consistent with X-ray photoemission spectroscopy as well as classical MD simulations employing polarizable potentials.[4] Although fluoride

† Part of the "Max Wolfsberg Festschrift".

* Corresponding author. E-mail: kuo2@llnl.gov.
‡ University of Pennsylvania.
§ Lawrence Livermore National Laboratory.

10.1021/jp808735x CCC: $40.75
Published on Web 01/27/2009

has been shown to be depleted at the surface, it can still be used as a model halide anion, representative of species that are of interest in the atmospheric community, such as chloride, bromide, or iodide.

Accordingly, in this study, we will look at the changes in structure, dynamics, and chemical reactivity at the liquid−vapor interface in the presence of a single fluoride anion. Counter ions, such as sodium, are neglected and replaced by a uniform neutralizing background because they are known to be depleted from the surface and thus unlikely to have a large effect on the properties of the liquid−vapor interface of interest here. The emphasis here will be on the effect of the anion on the electronic properties at the air−water interface.

II. Simulation Details

First principles MD simulations within the Born−Oppenheimer approximation were performed using the software suite CP2K wherein the needed energy and force was obtained from the QuickStep module.[30,31] The QuickStep module contains a fast electronic structure code based on the Kohn−Sham formulation of DFT.[32] For these calculations, a dual basis set of Gaussian type orbitals (TZV2P) with auxiliary plane waves expanded up to 280 Ry were utilized to describe the valence states. The core states are described through the Goedecker−Teter−Hutter pseudopotential.[33] This combination of basis sets and pseudopotentials has been validated to give converged properties for aqueous systems.[31] The present MD calculations were performed using the BLYP[23,24] exchange and correlation functionals due to its ubiquitous use in studies of aqueous systems. Simulations were carried out in the canonical ensemble using a time step of 0.48 fs. A Nosé−Hoover chain[34−36] of thermostats of length 3 were attached to every degree of freedom, with a time constant of 100 fs to ensure thermal equilibrium at 300 K over the entire simulation trajectory.

Five independent first principles MD simulations were performed using the slab configuration. Unlike previous liquid−vapor interface simulations, this study contains 215 water molecules plus one fluoride anion in a simulation cell of dimensions 15 Å × 15 Å × 71.44 Å. The choice of only one fluoride anion versus a high concentration of anions was made to clearly differentiate the changes to surface properties due to the presence of the anion, given a finite amount of computational resources. The size of the simulation cell in the z direction was chosen to ensure the decoupling of the two interfaces.[37] A total of five MD simulations were carried out with fluoride constrained to be at different interfacial depths of 0.0, 1.06, 2.12, 16.93, and 17.99 Å, respectively as measured from the center of the water slab. These values were chosen to adequately sample the fluoride anion at the two main target locations; namely, the bulk region (0.0, 1.06, and 2.12 Å) as well as near the Gibbs dividing surface (GDS) (16.93 and 17.99 Å). For simplicity, from this point forward we will refer to the two groups of simulations as SET_A and SET_B for the fluoride anion solvated in the bulk region of the water slab and near the GDS, respectively. Each simulation consists of 2 ps equilibration and a production run of 6 ps, except for the SET_B (17.99 Å) simulation, in which a 12 ps production run was used in the data analysis.

III. Results and Discussion

Density Profile. Large fluctuations in the density along the z axis are usually an early indicator of an unstable interfacial slab. Density profiles are shown in Figure 1. The density of the interfacial slab along the z axis was tabulated using 1-Å-wide bins. Best-fit density profiles using a hyperbolic tangent function are also shown based on the form

$$\rho(z) = \frac{1}{2}(\rho_l - \rho_v) - \frac{1}{2}(\rho_l - \rho_v)\tanh\left(\frac{z - z_{GDS}}{\delta}\right) \qquad (1)$$

Here, ρ_l and ρ_v correspond to the liquid and gas density, z_{GDS} is the location of the GDS, and δ is an interface thickness parameter. This same procedure has been used previously to characterize the neat air−water interface.[21] To improve statistics, the five independent MD simulations have been grouped into SET_A and SET_B as described above. Due to the limited time scale and finite size of our system, ρ_v was set to be zero explicitly in the fitting because no evaporation is observed. The resulting best-fit parameters are shown in Table 1. Both Figure 1 and the fitted parameter, ρ_l, for SET_A and SET_B show the interfacial slab to have a low density of 0.8 g/cm^3 in the bulk region when compared to the experimental density. The small difference in predicted liquid density (ρ_l) between SET_A and SET_B is within the statistical noise. A low predicted bulk density was also observed in other first principles simulations based on similar DFT schemes.[20,38] Thus, the present work reconfirms these prior results of a low density for aqueous systems obtained with different simulation codes, sampling methods, and ensembles.[20,39,40]

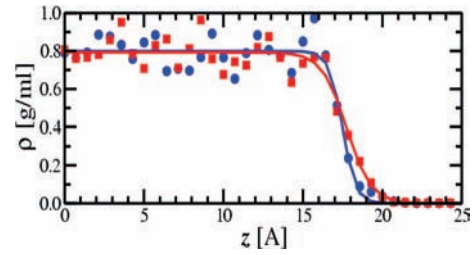

Figure 1. Density profiles for an aqueous liquid−vapor slab with fluoride. The three MD simulations in which the anions are in the bulk region (SET_A) are shown in blue and the two simulation representing fluoride near the GDS (SET_B) are shown in red. The GDSs are located at 17.49 and 17.75 Å for SET_A and SET_B, respectively.

TABLE 1: Fitted Density Profile Parameters for Liquid-Vapor Interface with Fluoride Situated at Different Depths[a]

	ρ_l (g/cm^3)	δ (Å)	z_{GDS} (Å)
SET_A	0.799	0.836	17.49
SET_B	0.792	1.547	17.75

[a] The density profile was fitted using $\rho(z) = (1)/(2)(\rho_l - \rho_v) - (1)/(2)(\rho_l - \rho_v)\tanh((z - z_{GDS})/(\delta))$ with the center of mass shifted to $z = 0$ Å for the fitting. A tabulation of all the fitted parameters from the simulations is also shown.

Although the interfacial thickness parameter, δ, is highly sensitive to the fitting procedure, the interfacial thickness for SET_A, 0.836 Å, is comparable to the value of 0.786 Å obtained previously for the neat air−water interface.[21] In the presence of an ion near the GDS, a value of 1.547 Å was obtained for SET_B. This increased interfacial thickness in the presence of an anion has also been observed previously.[41] Overall, there were no large fluctuations in the density profile, thus indicating stable interfaces. In addition, we can estimate the thickness of our interfacial slab after equilibration as 2 × z_{GDS}. Thus, for our MD simulations, the thickness are 35.0 and 35.5 Å for SET_A and SET_B, respectively.

Radial Distribution Functions. The radial distribution function (RDF) for fluoride−oxygen, $g_{FO}(r)$, and fluoride-hydrogen, $g_{FH}(r)$, are shown in Figure 2 for fluoride solvated in

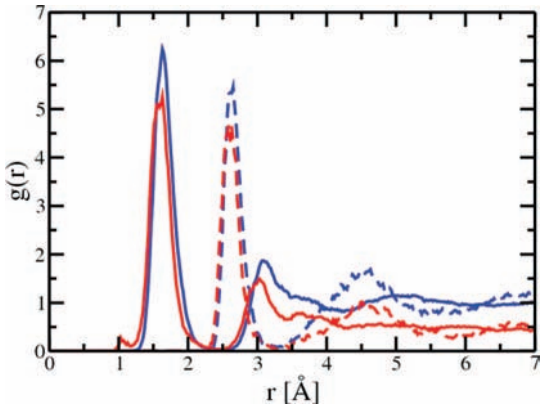

Figure 2. The radial distribution functions for fluoride-oxygen, $g_{FO}(r)$ and fluoride-hydrogen, $g_{FH}(r)$ are shown with dashed and solid lines, respectively. The RDFs were computed using a bin width of 0.02 Å. Results from SET_A are shown in blue, and results for SET_B are shown in red. Due to the symmetry of the interfacial slab, the computed $g_{FO}(r)$ and $g_{FH}(r)$ are expected to converge to 0.5 for SET_B.

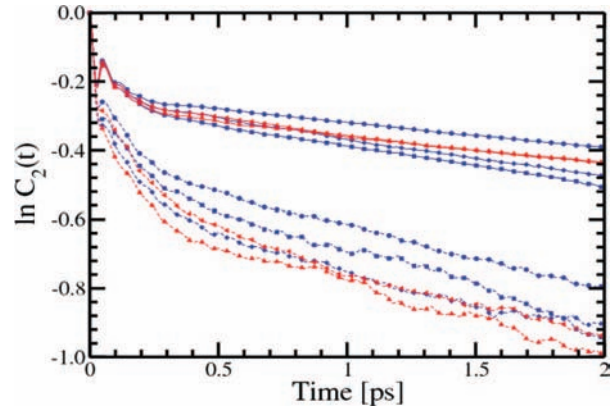

Figure 3. Second-order rotational correlation times, $C_2(t)$, for water in the bulk region and at the surface. Results from SET_A are shown in blue, and results for SET_B are shown in red. Each water slab has been partitioned into bulk and surface regions, which are shown using solid and dashed lines, respectively.

the bulk region and near the GDS, respectively. The computed coordination number (CN) is 4.1 for both fluorine−oxygen and fluorine−hydrogen for SET_A. The computed CN of 4.1 obtained here is in agreement with X-ray diffraction data (4.5 and 4.6) as well as QM/MM-based simulations.[42−44] Small angle neutron diffraction experiments show a CN that ranges from 5.2 to 6.9.[49] These inconsistencies between the interpretation of molecular structures from different experimental methods illustrates the difficulty of acquiring the coordination number in aqueous fluoride solutions.

Recent first principles MD simulations by Heuft and Meijer using DFT, albeit with different pseudopotentials and density, estimate the average residence time of water molecule in the first solvation shell of fluoride to be around 16 ps with a CN of ∼5.[45] With a long average residence time and low water mobility within the first solvation shell due to strong hydrogen bonding, a MD trajectory time scale on the order of several hundred picoseconds is necessary to adequately sample the solvation structure and produce a converged CN. Despite this caveat, the present computed solvation structure and CN for fluoride−oxygen are slightly different from the oxygen−oxygen CN of liquid water, thus indicating a slight perturbation of the hydrogen bond network due to the presence of fluorine. Importantly, the fluorine−oxygen and fluorine−hydrogen CN for SET_B are both 3.5.

Structurally, it was observed that fluorine is mostly bound to neighboring water in a tetrahedral geometry, in contrast to previous observations of a square pyramidal coordination structure.[45] Overall, the presence of fluoride results in a very well defined first solvation peak around 2.6 Å and minimum around 3.3 Å for both sets of $g_{FO}(r)$. Likewise, the $g_{FH}(r)$ RDF also shows a very well defined first solvation peak around 1.6 Å and first minimum around 2.5 Å. For both $g_{FO}(r)$ and $g_{FH}(r)$, we noticed a small decrease in the position of the first solvation peaks of 0.05 Å going from SET_A to SET_B. One interesting feature is the appearance of a small peak around 1.04 Å for $g_{FH}(r)$. This peak can be attributed to the fact that fluoride is the conjugate base of a weak acid and, thus, can form molecular hydrogen fluoride, which could account for the peak around 1.04 Å. The larger peak at 1.6 Å is due to the solvation of the fluoride anion by neighboring water molecules and can partially explain the slight peak shift observed on going from bulk to surface. Distinct RDFs for solvated F^- versus solvated molecular hydrogen fluoride has been observed previously from first principles MD simulation.[46−48] Although an exhaustive discussion of published RDFs obtained using first principles simulations on fluoride containing aqueous solution is not constructive due to the different simulation protocols as well as system simulated,[45−48] it should be noted that there are important differences that can be gleaned. In addition, another prominent difference is the peak height of the first solvation shell for $g_{FO}(r)$, for which we obtained a value of 5.5, which is closer to that observed from neutron diffraction data[49] and MD simulations carried out by Heuft and Meijer[45] than results of Sillanpaa et al.[46] The discrepancies between first principles simulation results can be due to the splitting of the first solvation peak, resulting in a lower but wider first solvation structure as well as use of different pseudopotentials, and simulation protocols. In addition, it should be noted that the use of experimental liquid density in prior studies versus the use of the slab geometry allows for the system to relax to its natural density and, thus, can also significantly alter the RDFs. Clearly, further MD simulation studies on aqueous fluoride would appear to be warranted.

Rotational Correlation Functions. The time correlation function, $C_2(t)$, was employed to monitor molecular reorientation of water molecules.

$$C_2(t - t_0) = \langle p_2[\vec{r}(t - t_0)\, \vec{r}(t_0); t]\rangle$$

Here, P_2 is the second Legendre polynomial, and the bisector for the H−O−H angle was chosen as the molecular vector, $\vec{r}$. The water slab was partitioned into two groups categorized, respectively, as "bulk" or "surface" regions by using an imaginary plane located at 2σ below the GDS as the cutoff. The correlation function, $C_2(t)$, shown in Figure 3, allows for the comparison of dynamic properties of individual water as a function of location. The salient feature of this plot is that there is a clear difference between the time correlation functions for water in the bulk region and that in the surface region. Systematically, the rotational dynamics for water appears to be faster for the surface region waters than for bulk region water; similar behavior has been observed previously for air−water and air−methanol interfaces.[21,22] From Figure 3, there appears to be no effective change in the rotational dynamics of water at the surface for SET_B that could be resolved from our simulation trajectory. Likewise, there appears to be no changes to $C_2(t)$ for water in the bulk region with and without the presence of fluoride anion.

Molecular Dipole Moments. Molecular dipole moments for the water and fluoride anion were computed via the Wannier

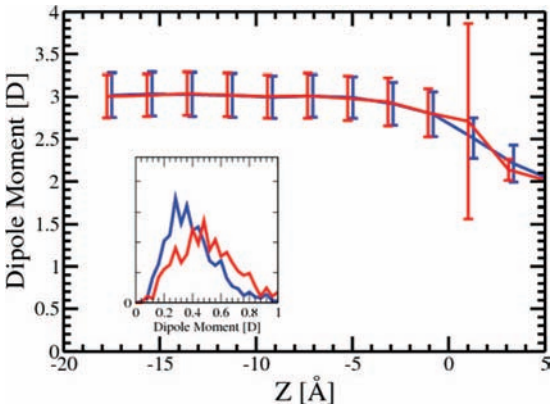

Figure 4. Molecular dipole moments for water and the standard deviation as a function of the slab depth. Results from SET_A are shown in blue, and results for SET_B are shown in red. The interfaces are shifted so that the GDS is located at 0.0 Å. The distributions of dipole moments for fluoride are shown in the inset.

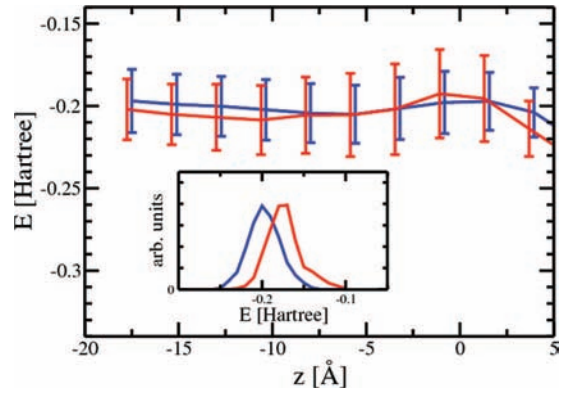

Figure 5. Effective HOMO energies for individual water molecules and standard deviation are plotted as a function of interfacial depth. Results from SET_A are shown in blue, and results for SET_B are shown in red. The HOMO energy distributions for fluoride are shown in the inset.

centroid analysis, in which we assume each molecule/ion to have four centers, with electronic charge centers reflecting the nature of the spin restricted calculation.[50,51] The average molecular dipole moment as a function of interfacial depth for water is shown in Figure 4. For both SET_A and SET_B, the average molecular dipole for water has the same qualitative behavior as observed for a neat air−water interface in which the average molecular dipole moments for water is around 3.0 D in the bulk region and decreases dramatically to a value around 2.0 D in the interfacial region.[20] This same qualitative trend has been seen in other liquid−vapor calculations using first principles simulations as well as polarizable empirical potentials.[21,22,52] From Figure 4, we conclude that the presence of fluoride in the bulk region has no direct influence on the molecular dipole of neighboring water, since SET_A and SET_B appear indistinguishable. This observation was also noted in previous solvated aqueous fluoride simulations.[45,53] With the propensity for the molecular dipole moments of water to decrease going from bulk to interface and previous observation that fluoride does not perturb the electronic structure of neighboring water, it would be expected that SET_A and SET_B should be indistinguishable near the GDS. Unlike the bulk region, the presence of fluoride near the GDS (SET_B) shows an increase in both the average molecular dipole and a substantial increase in the standard deviation. Since fluoride is still completely solvated near the GDS, as described above, the increase in molecular dipole is caused by anisotropy of the interface and not partial solvation of the first hydration shell, as seen for ion−water clusters.[53] As a result, the systematic shift toward a larger dipole moment for the fluoride anion is expected and is shown in the inset of Figure 4.

Molecular Electronic States. By utilizing the method developed by Vuilleumier and Sprik,[54] we have computed the effective highest occupied molecular orbital (HOMO) energies for each molecule (Figure 5). The effective HOMO energy distributions for fluoride in the bulk region and near the GDS are shown in the inset of Figure 5. For both the air−water and air−methanol interfaces, it was found that the average HOMO energies increase on going toward the interface. This indicates a reactive surface susceptible to electrophilic attacks.[20,22] Surprisingly, with the addition of a fluoride ion, it was found that the average HOMO energy for water is relatively constant as a function of interfacial depth. More interestingly, the HOMO energy for fluoride shows a shift of 0.025 H going from the bulk region to the surface region as seen in the inset of Figure 5. This shift makes the fluoride at the interface more susceptible to electrophilic attack than any other molecule and could explain why halides at the interface can dominate chemical reaction pathways.[18]

IV. Conclusions

Using first principles MD simulation, we have studied an embedded fluoride anion in a water slab to mimic bulk and interfacial solvation. Although there are unanswered questions regarding the density of hydrogen-bonded fluids using current DFT schemes, the use of the slab geometry does ensure that the present simulations were carried out at the natural equilibrium density for the adopted DFT approach. In the bulk region, we observed a tetrahedrally coordinated solvation structure around the fluoride with a coordination number around 4. A similar result obtains in the surface region of the water slab. These solvation structures and coordination numbers are in agreement with X-ray diffraction experiments and some other theoretical results but disagree with a recent analysis of small angle neutron diffraction data and other theoretical calculations, which suggest a significantly larger coordination number and Raman spectroscopy combined with ab initio calculations at the RHF/6-31+G* level,[55] which give CN ∼ 6. Specifically, Soper and Weckström analyzed their neutron diffraction data by employing an empirical potential structure refinement scheme.[56] In this way, they explored the nature of ionic hydration in KF solutions with different concentrations. Their results indicate that the coordination number is solute-concentration-dependent, changing from 6.9 (salt/water mole ratio of 1.2:100), to 5.2 (mole ratio of 4.8:100). Crystallography studies indicate fluoride ions to have octahedral coordination in $KF \cdot 4H_2O$[57] and tetrahedral coordination in $(n\text{-}C_4H_9)_4N^+F^- \cdot 32.8H_2O$,[58] which suggests that the nature of the cation could significantly affect the hydration state of F^-. As a result, one should perhaps be cautious when comparing the various experimental results to the simulation data.

In the present work, we found that there are small systematic shifts in the first solvation structure between the bulk and interfacial regions, as seen in the RDFs, as well as a small but finite propensity to form molecular hydrogen fluoride at the interface. Although small structural differences were observed, the effect of fluoride on the rotational dynamics of neighboring water is minimal, regardless of whether the anion is in the bulk or surface region of the water slab. The most dramatic changes in interfacial properties were electronic in nature when the ion

was present near the GDS. It was observed that the presence of fluoride near the GDS both increases and alters the molecular dipole moment distribution of neighboring water molecules, whereas such effects are not observed in the bulk region. As a result, the molecular dipole moment of the fluoride anion also increases near the GDS due to increased polarization of neighboring water molecules. Furthermore, the presence of the fluoride anion seems to alter the effective HOMO energies for water throughout the water slab. Unlike previous liquid−vapor interface studies in which interfacial molecules had higher energies and, thus, were more reactive in nature, the presence of fluoride in the water slab causes the potentially reactive sites to be shifted to the anion. Whether this behavior is representative of other halides is of great interest and can be elucidated in the future by utilizing the same type of simulations and analysis performed here for the fluoride anion. In addition, recent attempts to incorporate an atom-based, pairwise dispersion correction for different exchange and correlation functionals have yielded promising results for condensed-phase systems. If the same method is applied here, it will help quantify the role of London dispersion interactions at the liquid−vapor interface, where the effect will likely be more pronounced.

Acknowledgment. Part of this work was performed under the auspices of the U.S. Department of Energy by Lawrence Livermore National Laboratory under Contract DE-AC52-07NA27344. Computing resources were provided by Livermore Computing. We thank LLNL Computing staff for their help. M.H.H. thanks the National Institutes of Health (NIH) for their financial support.

References and Notes

(1) Ghosal, S.; Hemminger, J. C.; Bluhm, H.; Mun, B. S.; Hebenstreit, E. L. D.; Ketteler, G.; Ogletree, D. F.; Requejo, F. G.; Salmeron, M. *Science* **2005**, *307*, 563.

(2) Otten, D. E.; Petersen, P. B.; Saykally, R. J. *Chem. Phys. Lett.* **2007**, *449*, 261.

(3) Uejio, J. S.; Schwartz, C. P.; Duffin, A. M.; Drisdell, W. S.; Cohen, R. C.; Saykally, R. J. *Proc. Natl. Acad. Sci. U.S.A.* **2008**, *105*, 6809.

(4) Brown, M. A.; D'Auria, R.; Kuo, I. F. W.; Krisch, M. J.; Starr, D. E.; Bluhm, H.; Tobias, D. J.; Hemminger, J. C. *Phys. Chem. Chem. Phys.* **2008**, *10*, 4778.

(5) Soule, M. C. K.; Blower, P. G.; Richmond, G. L. *J. Phys. Chem. B* **2007**, *111*, 13703.

(6) Soule, M. C. K.; Blower, P. G.; Richmond, G. L. *J. Phys. Chem. A* **2007**, *111*, 3349.

(7) Gopalakrishnan, S.; Jungwirth, P.; Tobias, D. J.; Allen, H. C. *J. Phys. Chem. B* **2005**, *109*, 8861.

(8) Xu, M.; Larentzos, J. P.; Roshdy, M.; Criscenti, L. J.; Allen, H. C. *Phys. Chem. Chem. Phys.* **2008**, *10*, 4793.

(9) Jungwirth, P.; Tobias, D. J. *J. Phys. Chem. B* **2002**, *106*, 6361.

(10) Jungwirth, P.; Tobias, D. J. *Chem. Rev.* **2006**, *106*, 1259.

(11) Tobias, D. J.; Hemminger, J. C. *Science* **2008**, *319*, 1197.

(12) Yu, Y.; Ezell, M. J.; Zelenyuk, A.; Imre, D.; Alexander, L.; Ortega, J.; Thomas, J. L.; Gogna, K.; Tobias, D. J.; D'Anna, B.; Harmon, C. W.; Johnson, S. N.; Finlayson-Pitts, B. J. *Phys. Chem. Chem. Phys.* **2008**, *10*, 3063.

(13) Jungwirth, P.; Winter, B. *Annu. Rev. Phys. Chem.* **2008**, *59*, 343.

(14) Wick, C. D.; Dang, L. X. *Chem. Phys. Lett.* **2008**, *458*, 1.

(15) Cwiklik, L.; Buck, U.; Kulig, W.; Kubisiak, P.; Jungwirth, P. *J. Chem. Phys.* **2008**, *128*, 154306.

(16) Frigato, T.; VandeVondele, J.; Schmidt, B.; Schutte, C.; Jungwirth, P. *J. Phys. Chem. A* **2008**, *112*, 6125.

(17) Petersen, P. B.; Saykally, R. J. *Annu. Rev. Phys. Chem.* **2006**, *57*, 333.

(18) Knipping, E. M.; Lakin, M. J.; Foster, K. L.; Jungwirth, P.; Tobias, D. J.; Gerber, R. B.; Dabdub, D.; Finlayson-Pitts, B. J. *Science* **2000**, *288*, 301.

(19) Gard, E. E.; Kleeman, M. J.; Gross, D. S.; Hughes, L. S.; Allen, J. O.; Morrical, B. D.; Fergenson, D. P.; Dienes, T.; Galli, M. E.; Johnson, R. J.; Cass, G. R.; Prather, K. A. *Science* **1998**, *279*, 1184.

(20) Kuo, I. F. W.; Mundy, C. J. *Science* **2004**, *303*, 658.

(21) Kuo, I. F. W.; Mundy, C. J.; Eggimann, B. L.; McGrath, M. J.; Siepmann, J. I.; Chen, B.; Vieceli, J.; Tobias, D. J. *J. Phys. Chem. B* **2006**, *110*, 3738.

(22) Kuo, I. F. W.; Mundy, C. J.; McGrath, M. J.; Siepmann, J. I. *J. Phys. Chem. C* **2008**, *112*, 15412.

(23) Becke, A. D. *Phys. Rev. A* **1988**, *38*, 3098.

(24) Lee, C.; Yang, W.; Parr, R. G. *Phys. Rev. B* **1988**, *37*, 785.

(25) Perdew, J. P.; Burke, K.; Ernzerhof, M. *Phys. Rev. Lett.* **1996**, *77*, 3865.

(26) Kohanoff, J. *Electronic structure calculations for solids and molecules: theory and computational methods*; Cambridge University Press: Cambridge, U.K.; New York, 2006.

(27) Thonhauser, T.; Cooper, V. R.; Li, S.; Puzder, A.; Hyldgaard, P.; Langreth, D. C. *Phys. Rev. B* **2007**, *76*.

(28) Tobias, D. J.; Jungwirth, P.; Parrinello, M. *J. Chem. Phys.* **2001**, *114*, 7036.

(29) Jungwirth, P.; Curtis, J. E.; Tobias, D. J. *Chem. Phys. Lett.* **2003**, *367*, 704.

(30) CP2K. http://cp2k.berlios.de.

(31) VandeVondele, J.; Krack, M.; Mohamed, F.; Parrinello, M.; Chassaing, T.; Hutter, R. *Comput. Phys. Commun.* **2005**, *167*, 103.

(32) Lippert, G.; Hutter, J.; Parrinello, M. *Mol. Phys.* **1997**, *92*, 477.

(33) Goedecker, S.; Teter, M.; Hutter, J. *Phys. Rev. B* **1996**, *54*, 1703.

(34) Nosé, S. *J. Chem. Phys.* **1984**, *81*, 511.

(35) Hoover, W. G. *Phys. Rev. A* **1985**, *31*, 1695.

(36) Martyna, G. J.; Klein, M. L.; Tuckerman, M. *J. Chem. Phys.* **1992**, *97*, 2635.

(37) Mundy, C. J.; Kuo, I. F. W. *Chem. Rev.* **2006**, *106*, 1282.

(38) McGrath, M. J.; Siepmann, J. I.; Kuo, I. F. W.; Mundy, C. J.; VandeVondele, J.; Hutter, J.; Mohamed, F.; Krack, M. *ChemPhysChem* **2005**, *6*, 1894.

(39) Kuo, I. F. W.; Mundy, C. J.; McGrath, M. J.; Siepmann, J. I.; VandeVondele, J.; Sprik, M.; Hutter, J.; Chen, B.; Klein, M. L.; Mohamed, F.; Krack, M.; Parrinello, M. *J. Phys. Chem. B* **2004**, *108*, 12990.

(40) McGrath, M. J.; Siepmann, J. I.; Kuo, I. F. W.; Mundy, C. J.; VandeVondele, J.; Hutter, J.; Mohamed, F.; Krack, M. *J. Phys. Chem. A* **2006**, *110*, 640.

(41) Warren, G. L.; Patel, S. *J. Phys. Chem. B* **2008**, *112*, 11679.

(42) Terekhova, D. S.; Ryss, A. I.; Radchenko, I. V. *J. Struct. Chem.* **1970**, *10*, 807.

(43) Ohrn, A.; Karlstrom, G. *J. Phys. Chem. B* **2004**, *108*, 8452.

(44) Tongraar, A.; Rode, B. M. *Phys. Chem. Chem. Phys.* **2003**, *5*, 357.

(45) Heuft, J. M.; Meijer, E. J. *J. Chem. Phys.* **2005**, *122*, 094501.

(46) Sillanpaa, A. J.; Simon, C.; Klein, M. L.; Laasonen, K. *J. Phys. Chem. B* **2002**, *106*, 11315.

(47) Simon, C.; Klein, M. L. *ChemPhysChem* **2005**, *6*, 148.

(48) Laasonen, K.; Larrucea, J.; Sillapaa, A. *J. Phys. Chem. B* **2006**, *110*, 12699.

(49) Soper, A. K.; Weckstrom, K. *Biophys. Chem.* **2006**, *124*, 180.

(50) Berghold, G.; Mundy, C. J.; Romero, A. H.; Hutter, J.; Parrinello, M. *Phys. Rev. A* **2000**, *61*, 10040.

(51) Silvestrelli, P. L.; Parrinello, M. *Phys. Rev. Lett.* **1999**, *82*, 3308.

(52) Wick, C. D.; Kuo, I. F. W.; Mundy, C. J.; Dang, L. X. *J. Comput. Theor. Chem.* **2007**, *3*, 2002.

(53) Krekeler, C.; Hess, B.; Delle Site, L. *J. Chem. Phys.* **2006**, *125*, 054305.

(54) Vuilleumier, R.; Sprik, M. *J. Chem. Phys.* **2001**, *115*, 3454.

(55) Craig, J. D. C.; Brooker, M. H. *J. Solution Chem.* **2000**, *29*, 879.

(56) Soper, A. K. *Phys. Rev. B* **2005**, *72*, 104204.

(57) Beurskens, G.; Jeffrey, G. A. *J. Chem. Phys.* **1964**, *41*, 917.

(58) McMullan, R. K.; Bonamico, M.; Jeffrey, G. A. *J. Chem. Phys.* **1963**, *39*, 3295.

JP808735X